2017

Mid-Infrared Self-Similar Compression of Picosecond Pulse in an Inversely Tapered Silicon Ridge Waveguide

Jin-Hui Yuan
Beijing University of Posts and Telecommunications

Jian Chen
Beijing University of Posts and Telecommunications, Beijing

Feng Li
The Hong Kong Polytechnic University

See next page for additional authors

Recommended Citation

Farrell, G., Chen, J. & Yuan, J. (2017). Mid-Infrared Self-Similar Compression of Picosecond Pulse in an Inversely Tapered Silicon Ridge Waveguide. *Optics Express*, vol. 25, no. 26, pp. 33439-33450. doi.org/10.1364/OE.25.033439

Research Article | Vol. 25, No. 26 | 25 Dec 2017 | OPTICS EXPRESS 33439
Optics EXPRESS

Mid-infrared self-similar compression of picosecond pulse in an inversely tapered silicon ridge waveguide

JINHUI YUAN,[1,2,3] JIAN CHEN,[1] FENG LI,[2,3,*] CHAO MEI,[1,3] ZHE KANG,[3] XIANTING ZHANG,[3] YIN XU,[3] BINBIN YAN,[1] XINZHU SANG,[1] QIANG WU,[4] XIAN ZHOU,[3] KANGPING ZHONG,[3] KUIRU WANG,[1] CHONGXIU YU,[1] GERALD FARRELL,[5] AND P. K. A. WAI[3]

[1]*State Key Laboratory of Information Photonics and Optical Communications, Beijing University of Posts and Telecommunications, Beijing 100876, China*
[2]*The Hong Kong Polytechnic University Shenzhen Research Institute, Shenzhen 518057, China*
[3]*Photonics Research Centre, Department of Electronic and Information Engineering, the Hong Kong Polytechnic University, Hong Kong SAR, China*
[4]*Department of Physics and Electrical Engineering, Northumbria University, Newcastle upon Tyne, NE1 8ST, UK*
[5]*Photonics Research Centre, Dublin Institute of Technology, Dublin, Ireland*
**enlf@polyu.edu.hk*

Abstract: On chip high quality and high degree pulse compression is desirable in the realization of integrated ultrashort pulse sources, which are important for nonlinear photonics and spectroscopy. In this paper, we design a simple inversely tapered silicon ridge waveguide with exponentially decreasing dispersion profile along the propagation direction, and numerically investigate self-similar pulse compression of the fundamental soliton within the mid-infrared spectral region. When higher-order dispersion (HOD), higher-order nonlinearity (HON), losses (α), and variation of the Kerr nonlinear coefficient $\gamma(z)$ are considered in the extended nonlinear Schrödinger equation, a 1 ps input pulse at the wavelength of 2490 nm is successfully compressed to 57.29 fs in only 5.1-cm of propagation, along with a compression factor F_c of 17.46. We demonstrated that the impacts of HOD and HON are minor on the pulse compression process, compared with that of α and variation of $\gamma(z)$. Our research results provide a promising solution to realize integrated mid-infrared ultrashort pulse sources.

OCIS codes: (130.0250) Optoelectronics; (190.4390) Nonlinear optics, integrated optics; (320.5520) Pulse compression.

References and links

1. J. W. Nicholson, A. D. Yablon, M. F. Yan, P. Wisk, R. Bise, D. J. Trevor, J. Alonzo, T. Stockert, J. Fleming, E. Monberg, F. Dimarcello, and J. Fini, "Coherence of supercontinua generated by ultrashort pulses compressed in optical fibers," Opt. Lett. **33**(18), 2038–2040 (2008).
2. Q. Li, J. N. Kutz, and P. K. A. Wai, "High-degree pulse compression and high-coherence supercontinuum generation in a convex dispersion profile," Opt. Commun. **301–302**, 29–33 (2013).
3. F. Li, Q. Li, J. Yuan, and P. K. A. Wai, "Highly coherent supercontinuum generation with picosecond pulses by using self-similar compression," Opt. Express **22**(22), 27339–27354 (2014).
4. J. H. Yuan, Z. Kang, F. Li, X. T. Zhang, X. Z. Sang, Q. Wu, B. B. Yan, K. R. Wang, X. Zhou, K. P. Zhong, G. Y. Zhou, C. X. Yu, C. Lu, H. Y. Tam, and P. K. A. Wai, "Mid-infrared octave-spanning supercontinuum and frequency comb generation in a suspended germanium-membrane ridge waveguide," J. Lightwave Technol. **35**(14), 2994–3002 (2017).
5. Yu. S. Kivshar and G. P. Agraval, *Optical solitons: from fibers to photonic crystals*, (Academic, 2003).
6. I. V. Dzedolik and A. I. Dzedolik, "Soliton formation from a Gaussian pulse in an optical fiber," Tech. Phys. **47**(6), 713–719 (2002).
7. G. P. Agrawal, *Applications of Nonlinear Fiber Optics*, 2nd ed. (Elsevier, 2007).
8. T. Südmeyer, F. Brunner, E. Innerhofer, R. Paschotta, K. Furusawa, J. C. Baggett, T. M. Monro, D. J. Richardson, and U. Keller, "Nonlinear femtosecond pulse compression at high average power levels by use of a large-mode-area holey fiber," Opt. Lett. **28**(20), 1951–1953 (2003).

#308036 https://doi.org/10.1364/OE.25.033439
Journal © 2017 Received 27 Sep 2017; revised 12 Nov 2017; accepted 13 Nov 2017; published 22 Dec 2017

Optics EXPRESS

9. K. F. Mak, J. C. Travers, N. Y. Joly, A. Abdolvand, and P. S. J. Russell, "Two techniques for temporal pulse compression in gas-filled hollow-core kagomé photonic crystal fiber," Opt. Lett. **38**(18), 3592–3595 (2013).
10. K. C. Chan and H. F. Liu, "Short Pulse Generation by Higher Order Soliton-Effect Comression: Effects of Optical Fiber Characteristics," IEEE J. Quantum Electron. **31**, 2226–2235 (1995).
11. M. D. Pelusi and H. F. Liu, "Higher order soliton pulse compression in dispersion-decreasing optical fibers," IEEE J. Quantum Electron. **33**, 1430–1439 (1997).
12. Q. Li, J. N. Kutz, and P. K. A. Wai, "Cascaded higher-order soliton for non-adiabatic pulse compression," J. Opt. Soc. Am. B **27**(11), 2180–2189 (2010).
13. A. C. Peacock, "Mid-IR soliton compression in silicon optical fibers and fiber tapers," Opt. Lett. **37**(5), 818–820 (2012).
14. S. V. Chernikov, E. M. Dianov, D. J. Richardson, and D. N. Payne, "Soliton pulse compression in dispersion-decreasing fiber," Opt. Lett. **18**(7), 476–478 (1993).
15. M. L. V. Tse, P. Horak, J. H. V. Price, F. Poletti, F. He, and D. J. Richardson, "Pulse compression at 1.06 μm in dispersion-decreasing holey fibers," Opt. Lett. **31**(23), 3504–3506 (2006).
16. J. C. Travers, J. M. Stone, A. B. Rulkov, B. A. Cumberland, A. K. George, S. V. Popov, J. C. Knight, and J. R. Taylor, "Optical pulse compression in dispersion decreasing photonic crystal fiber," Opt. Express **15**(20), 13203–13211 (2007).
17. J. Hu, B. S. Marks, C. R. Menyuk, J. Kim, T. F. Carruthers, B. M. Wright, T. F. Taunay, and E. J. Friebele, "Pulse compression using a tapered microstructure optical fiber," Opt. Express **14**(9), 4026–4036 (2006).
18. P. J. Roberts, B. J. Mangan, H. Sabert, F. Couny, T. A. Birks, J. C. Knight, and P. St. J. Russell, "Control of dispersion in photonic crystal fibers," Opt. Fiber Commun. Rep. **2**(5), 435–461 (2005).
19. V. I. Kruglov, A. C. Peacock, and J. D. Harvey, "Exact self-similar solutions of the generalized nonlinear Schrödinger equation with distributed coefficients," Phys. Rev. Lett. **90**(11), 113902 (2003).
20. V. I. Kruglov, A. C. Peacock, and J. D. Harvey, "Exact solutions of the generalized nonlinear Schrödinger equation with distributed coefficients," Phys. Rev. E Stat. Nonlin. Soft Matter Phys. **71**(5 Pt 2), 056619 (2005).
21. K. Senthilnathan, K. Nakkeeran, Q. Li, and P. K. A. Wai, "Pedestal free pulse compression of chirped optical solitons," Opt. Commun. **285**(6), 1449–1455 (2012).
22. D. Méchin, S. H. Im, V. I. Kruglov, and J. D. Harvey, "Experimental demonstration of similariton pulse compression in a comblike dispersion-decreasing fiber amplifier," Opt. Lett. **31**(14), 2106–2108 (2006).
23. C. Mei, F. Li, J. H. Yuan, Z. Kang, X. T. Zhang, K. R. Wang, X. Z. Sang, Q. Wu, B. B. Yan, X. Zhou, L. Wang, C. X. Yu, and P. K. A. Wai, "High degree picosecond pulse compression in chalcogenide-silicon slot waveguide taper," J. Lightwave Technol. **34**(16), 3843–3852 (2016).
24. L. Zhang, A. M. Agarwal, L. C. Kimerling, and J. Michel, "Nonlinear Group IV photonics based on silicon and germanium: from near-infrared to mid-infrared," Nanophotonics **3**(4–5), 247–268 (2014).
25. R. Dekker, N. Usechak, M. Forst, and A. Driessen, "Ultrafast nonlinear all-optical processes in silicon-on-insulator waveguides," J. Phys. D Appl. Phys. **40**(14), 249–271 (2007).
26. Q. Lin, O. J. Painter, and G. P. Agrawal, "Nonlinear optical phenomena in silicon waveguides: modeling and applications," Opt. Express **15**(25), 16604–16644 (2007).
27. R. M. Osgood, N. C. Panoiu, J. I. Dadap, X. Liu, X. Chen, I. W. Hsieh, E. Dulkeith, W. M. J. Green, and Y. A. Vlasov, "Engineering nonlinearities in nanoscale optical systems: physics and applications in dispersion-engineered silicon nanophotonic wires," Adv. Opt. Photonics **1**(1), 162–235 (2009).
28. J. Leuthold, C. Koos, and W. Freude, "Nonlinear silicon photonics," Nat. Photonics **4**(8), 535–544 (2010).
29. L. Yin and G. P. Agrawal, "Impact of two-photon absorption on self-phase modulation in silicon waveguides," Opt. Lett. **32**(14), 2031–2033 (2007).
30. S. Pearl, N. Rotenberg, and H. M. van Driel, "Three photon absorption in silicon for 2300-3300 nm," Appl. Phys. Lett. **93**(13), 131102 (2008).
31. Z. Wang, H. Liu, N. Huang, Q. Sun, J. Wen, and X. Li, "Influence of three-photon absorption on mid-infrared cross-phase modulation in silicon-on-sapphire waveguides," Opt. Express **21**(2), 1840–1848 (2013).
32. D. C. Harris, "Durable 3-5 μm transmitting infrared window materials," Infrared Phys. Technol. **39**(4), 185–201 (1998).
33. Y. Yue, L. Zhang, H. Huang, R. G. Beausoleil, and A. E. Willner, "Silicon-on-nitride waveguide with ultralow dispersion over an octave-spanning mid-infrared wavelength range," IEEE Photonics J. **4**(1), 126–132 (2012).
34. B. Kuyken, X. Liu, R. M. Osgood, R. Baets, G. Roelkens, and W. M. Green, "Mid-infrared to telecom-band supercontinuum generation in highly nonlinear silicon-on-insulator wire waveguides," Opt. Express **19**(21), 20172–20181 (2011).
35. X. Liu, R. M. Osgood, Y. A. Vlasov, and W. M. J. Green, "Mid-infrared optical parametric amplifier using silicon nanophotonic waveguides," Nat. Photonics **4**(8), 557–560 (2010).
36. N. Singh, D. D. Hudson, Y. Yu, C. Grillet, S. D. Jackson, A. Casas-Bedoya, A. Read, P. Atanackovic, S. G. Duvall, S. Palomba, B. Luther-Davies, S. Madden, D. J. Moss, and B. J. Eggleton, "Midinfrared supercontinuum generation from 2 to 6 μm in a silicon nanowire," Optica **2**(9), 797–802 (2015).
37. R. K. W. Lau, M. R. E. Lamont, A. G. Griffith, Y. Okawachi, M. Lipson, and A. L. Gaeta, "Octave-spanning mid-infrared supercontinuum generation in silicon nanowaveguides," Opt. Lett. **39**(15), 4518–4521 (2014).
38. S. A. Akhmanov, V. A. Vysloukh, and A. S. Chirkin, "Self-action of wave packets in a nonlinear medium and femtosecond laser pulse generation," Phys. Uspekhi **29**(7), 642–647 (1986).

Optics EXPRESS

39. L. Yin, Q. Lin, and G. P. Agrawal, "Soliton fission and supercontinuum generation in silicon waveguides," Opt. Lett. **32**(4), 391–393 (2007).
40. R. Soref, S. J. Emelett, and W. Buchwald, "Silicon waveguided components for the long-wave infrared region," J. Opt. A, Pure Appl. Opt. **8**(10), 840–848 (2006).
41. K. Bergman, L. P. Carloni, A. Biberman, J. Chan, and G. Hendry, *Photonic Network-on-chip Design* (Springer, 2014).
42. G. Li, J. Yao, H. Thacker, A. Mekis, X. Zheng, I. Shubin, Y. Luo, J.-H. Lee, K. Raj, J. E. Cunningham, and A. V. Krishnamoorthy, "Ultralow-loss, high-density SOI optical waveguide routing for macrochip interconnects," Opt. Express **20**(11), 12035–12039 (2012).
43. S. Lavdas, J. B. Driscoll, R. R. Grote, R. M. Osgood, and N. C. Panoiu, "Pulse compression in adiabatically tapered silicon photonic wires," Opt. Express **22**(6), 6296–6312 (2014).
44. K. Senthilnathan, Q. Li, K. Nakkeeran, and P. K. A. Wai, "Robust pedestal-free pulse compression in cubic-quintic nonlinear media," Phys. Rev. A **78**, 033835 (2008).
45. P. Dong, W. Qian, S. Liao, H. Liang, C.-C. Kung, N.-N. Feng, R. Shafiiha, J. Fong, D. Feng, A. V. Krishnamoorthy, and M. Asghari, "Low loss shallow-ridge silicon waveguides," Opt. Express **18**(14), 14474–14479 (2010).
46. M. Borselli, T. Johnson, and O. Painter, "Beyond the Rayleigh scattering limit in high-Q silicon microdisks: theory and experiment," Opt. Express **13**(5), 1515–1530 (2005).

1. Introduction

Optical pulse compression technique is important for many applications, including optical communication, nonlinear microscopy, supercontinuum and frequency comb generations [1–6], etc. In laser systems, prism or grating-based compressors are typically used to compensate the linear chirp of pulses to compress them [7–9]. But the compression factor of linear chirp compensation is limited especially when the chirp is not significant and the pulse spectrum is not wide. Several nonlinear pulse compression schemes have been used to compress the pulse width with spectral broadening. In anomalous dispersion region, the breathing of higher-order solitons can be used to compress the pulse without grating pairs, but significant pedestal will accompany the compressed pulse and the compression factor is not high [9–13]. Adiabatic soliton compression in a dispersion decreasing fiber can provide a high compression factor without generating significant pedestal [14,15]. But the long fiber length required is undesirable in most systems because of compactness and cost [16–18]. Compared with the adiabatic compression, self-similar pulse compression can achieve large compression factor without pedestal generation in much shorter nonlinear media [3,19–23]. In a 6.4 m nonlinearity increasing photonic crystal fiber (PCF) taper, a 1 ps pulse is self-similarly compressed to 53.6 fs with low pedestal [3]. However, the required peak power of the input pulse reaches several kilowatts, and such PCF tapers with specific taper profiles are still difficult to fabricate in the fiber drawing process. Compared with the dynamic control required in the drawing of a fiber taper, controlling the waveguide dimension of on-chip devices is much easier. Self-similar compression of a pulse from 1 ps to 81.5 fs in a 6 cm long dispersion decreasing chalcogenide slot waveguide taper has been demonstrated by simulation [23]. However, further compression under the self-similar scheme in such a slot waveguide is limited by the two-photon absorption (TPA) of the substrate material and higher-order dispersion (HOD).

Compared with the PCF, silicon waveguide has much stronger Kerr nonlinearity. More important, silicon waveguide is CMOS compatible [24], which is easier to be fabricated than chalcogenide slot waveguide. Adopting silicon waveguide will greatly promote the development of on-chip scale nonlinear photonics [25–28]. In the near-infrared spectral region around 1.55 μm, the TPA in silicon has a significant effect [23,29], which greatly limits the output optical power and degrades the efficiency of nonlinear optical processes. TPA can be greatly reduced in the mid-infrared spectral region. Silicon waveguide has no TPA beyond 2.2 μm, and three-photon absorption (3PA) can be significantly reduced when the intensity of pulse is below 2.22 GW/cm^2 [30,31]. The transmission window of silicon for nonlinear applications without TPA is in the wavelength range of 2.2 to 8.5 μm [24,32]. With the development of various devices including laser sources and passive components in the

mid-infrared region in the past decade, silicon-based mid-infrared photonics has attracted much more interest in recent years [33–35].

In this paper, we propose an inversely tapered silicon ridge waveguide with a simple taper profile to realize exponentially decreasing dispersion profile for self-similar pulse compression. By increasing the waveguide width, the dispersion of the waveguide is gradually reduced. The nonlinear evolution in the waveguide taper of a chirped soliton pulse with a wavelength of 2490 nm is investigated with a generalized nonlinear Schrödinger equation (GNLSE). The paper is organized as follows. In Section 2, the GNLSE and the principle of self-similar compression in the waveguide taper will be introduced. In Section 3, we design and characterize the dispersion and nonlinear feature of the proposed silicon waveguide taper. The self-similar pulse compression of chirped fundamental soliton in the waveguide taper is numerically investigated in Section 4. Finally we draw conclusions in Section 5.

2. Theoretical model and principle of self-similar pulse compression

The propagation of optical pulses in parameters varying silicon waveguide can be modeled by the GNLSE which includes the HOD and higher-order nonlinearity (HON) [36–38] as following

$$\frac{\partial A}{\partial z}=\sum_{\mathrm{m}\geq 2}\frac{i^{\mathrm{m}+1}\beta_{\mathrm{m}}(z)}{\mathrm{m}!}\frac{\partial^{\mathrm{m}}A}{\partial t^{\mathrm{m}}}+i\gamma(z)\left(1+i\tau_{s}\frac{\partial}{\partial t}\right)\left|A\right|^{2}A-\frac{1}{2}\alpha_{0}A-\frac{\gamma_{3\mathrm{PA}}}{3A_{\mathrm{eff}}^{2}(z)}\left|A\right|^{4}A, \quad (1)$$

where $A(z, t)$ is the slowly varying envelope. $\beta_{\mathrm{m}}(z)$ (m = 1, 2, …, and 6) is the m-th order dispersion coefficient at propagation distance z and obtained by Taylor expansion of the propagation constant $\beta(\omega)$ at a specific wavelength. $\tau_{\mathrm{s}} = 1/\omega_0$ is the shock time to describe the self-steepening, where ω_0 is the actual frequency of the optical carrier. $\gamma(z)$ represents the Kerr nonlinear coefficient varying along z, which is calculated by integration over the whole cross-section of the waveguide as [23,39]

$$\gamma=\frac{\omega}{c}\frac{\iint n_{2}(x,y)\left|F(x,y)\right|^{4}dxdy}{(\iint\left|F(x,y)\right|^{2}dxdy)^{2}}, \quad (2)$$

where $n_2(x, y)$ and $F(x, y)$ represent the distributions of nonlinear Kerr index and the electric field, respectively. The varying cross-section of the waveguide along propagation direction will lead to a varying $\gamma(z)$. The delayed Raman response is negligible in silicon and therefore no included [36,37]. α_0 represents the linear loss of the waveguide. Since silicon has very low TPA in the spectral region >2.2 μm, we can neglect TPA when the pump wavelength is chosen as 2490 nm [30,31]. $\gamma_{3\mathrm{PA}}$ represents the 3PA coefficient. $A_{\mathrm{eff}}(z)$ is the effective mode area of the light at different taper position z. In the spectral region from 2200 to 3200 nm, 3PA plays an important role [36]. The impact of nonlinear loss induced by 3PA depends on the optical intensity in the waveguide [24,30,31].

It is known that self-similar solutions can be found for parameters varying nonlinear Schrödinger equation (NLSE) [3,23]

$$\frac{\partial A}{\partial z}=-\frac{i\beta_{2}(z)}{2}\frac{\partial^{2}A}{\partial t^{2}}+i\gamma(z)\left|A\right|^{2}A, \quad (3)$$

when the nonlinear coefficient $\gamma(z)$ is a constant and dispersion profile $\beta_2(z)$ varies exponentially along the waveguide taper as

$$\beta_{2}(z)=\beta_{2}(0)\exp(-\sigma z), \quad (4)$$

Optics EXPRESS

where $\sigma = \beta_2(0)\xi$ and ξ is the initial chirp factor of the input pulse. The analytic self-similar solution [19–21] of Eq. (3) is given by [3,23]

$$A(z,t) = \left(P_0 e^{\sigma z}\right)^{1/2} \operatorname{sech}\left[\frac{(t-t_0)e^{\sigma z}}{T_0}\right] \exp\left[\frac{i}{2}\xi(t-t_0)^2 e^{\sigma z}\right], \tag{5}$$

$$P_0 = \left|\beta_2(0)\right| \Big/ \left[\gamma(0) T_0^2\right], \tag{6}$$

where T_0 and P_0 are the pulse width and peak power at $z = 0$, respectively. t_0 is the temporal position of the pulse peak. As shown in Eq. (5), the duration and peak power of the pulse will decrease and increase exponentially along z, respectively. As the pulse compression factor only depends on the ratio of $\beta_2(z)$ and $\beta_2(0)$, a suitable waveguide design to realize a large ratio of the dispersion at the output and input points is the key for self-similar pulse compression.

3. Design of silicon ridge waveguide taper

To design a silicon ridge waveguide that satisfies the self-similar compression condition as described in Eq. (4), we first characterize the silicon ridge waveguide with different width as shown in Fig. 1(a). The waveguide is fabricated on silicon on insulator (SOI) wafer. After the etching of the silicon layer with thickness H_1, the silica substrate is also etched for a depth of H_2 with the same pattern of the silicon layer. The over etching into the silica layer will reduce the light in the silica layer thus enhance the refractive index contrast and confinement of light in the waveguide. Even for the light penetrating into the silica layer, the attenuation will not be high since the pump wavelength is still within the transparency window of silica [24,40]. The open surfaces of the waveguide are surrounded by air. The height of the silicon layer (H_1) and the thin silica layer (H_2) are 320 nm and 150 nm, respectively. The waveguide widths at the input (W_{in}) and output (W_{out}) ports are 800 and 1390 nm, respectively.

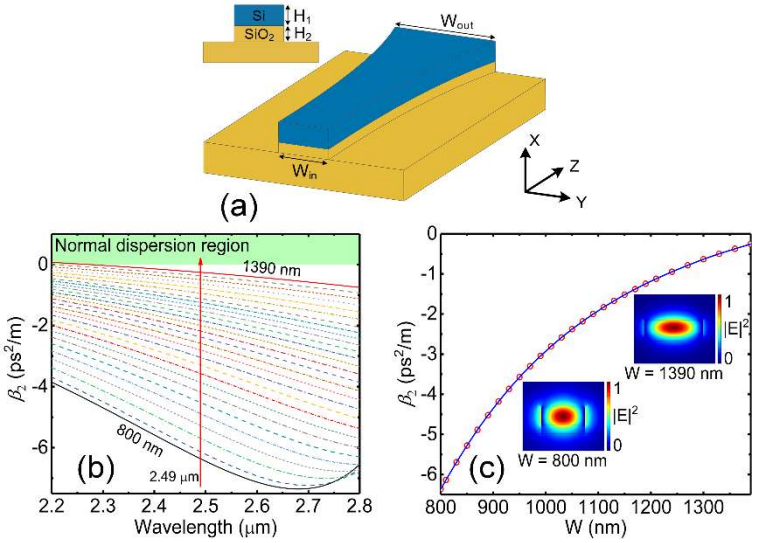

Fig. 1. (a) Schematic diagram of the designed inversely tapered silicon ridge waveguide. (b) Dispersion curves of the fundamental mode in the designed waveguide with width (W) varying from 800 to 1390 nm. The red vertical line indicates the pump wavelength of 2490 nm and the light green region has normal dispersion. (c) The variation of β_2 at 2490 nm versus W. The insets show the mode patterns at the input and output ports of the waveguide taper.

The dispersion and nonlinear coefficients of the fundamental mode at different W are characterized with finite element method (FEM). Figure 1(b) shows the dispersion curves of

Optics EXPRESS

the fundamental mode in waveguide with different W. When W increases, the minimum of the dispersion curve is shifted towards longer wavelength. In the design of dispersion decreasing waveguide taper in [23], the operation points were chosen on the longer wavelength side with respect to the minimum points of the dispersion curves since the dispersion curve on the shorter wavelength side is insensitive to the taper size in that design. In this work, the shorter wavelength side with respect to the minimum points of the dispersion curves significantly shifts upwards with the increase of W. In [23], the third-order dispersion increases significantly along the decrease of $|\beta_2|$ and the zero-dispersion wavelength (ZDW) is very close to the pump wavelength 1550 nm at the end of the taper, which distorts the soliton in the propagation. In our design, the third-order dispersion decreases along the decrease of $|\beta_2|$ and the value of $|\beta_3|$ is much lower than that in [23]. The ZDW is far away from the pump wavelength 2490 nm in the whole taper. For the black solid curve in Fig. 1(b), the minimum of the dispersion occurs at 2680 nm. Other dispersion curves shown in Fig. 1(b) are similar to the black solid one. When W increases, the value of β_2 at the pump wavelength 2490 nm increases as shown by the red vertical line in Fig. 1(b). Figure 1(c) shows the variation of β_2 at 2490 nm versus W. The circles are the β_2 values calculated by FEM and the solid curve is the spline interpolation. The insets of Fig. 1(c) show the mode patterns at the input and output ports of the waveguide taper for the light with a wavelength of 2490 nm. From Fig. 1(c), when W increases from 800 to 1390 nm, β_2 increases monotonically from –6.3628 to –0.2584 ps^2/m, where the ratio of the two β_2 values is 24.62. The signal wavelength can be selected from a rather broad range because of the gentle slopes of the dispersion curves in Fig. 1(b). Variation in the central wavelength will change the start and end values of β_2, which will slightly change the compression ratio. The gentle slopes of the dispersion curves significantly reduce the sensitivity of the pulse compression to wavelength detune after the fabrication of the waveguide taper.

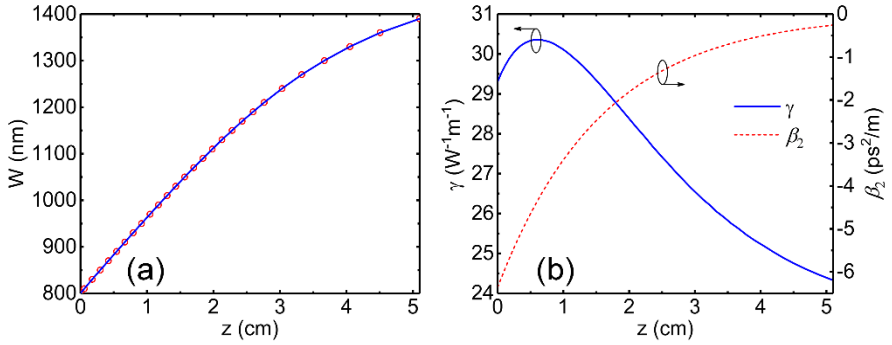

Fig. 2. (a) The profile of $W(z)$ along the propagation direction z. (b) The variations of the nonlinearity coefficient $\gamma(z)$ (blue solid curve) and dispersion β_2 (red dashed curve) along z.

With the $\beta_2(W)$ shown in Fig. 1(c), Fig. 2(a) shows the taper profile $W(z)$ that can fulfill the self-similar compression condition. The circles and solid curve in Fig. 2(a) correspond to those in Fig. 1(c). When the waveguide is tapered, it is not possible to keep the nonlinear coefficient $\gamma(z)$ constant, thus the nonlinear coefficient γ will also be changed with the variation of W. The nonlinear indices n_2 of silicon and silica are 4.79×10^{-18} m^2/W [24] and 2.20×10^{-20} m^2/W, respectively. The electrical field distributions in both the silicon and silica regions are considered in the calculation of γ. Figure 2(b) shows the variations of γ versus z besides the exponentially decreasing dispersion curve at 2490 nm. The taper length is 5.1 cm. From Fig. 2(b), the variation of $\gamma(z)$ (blue solid curve) is not monotonic. The value of γ increases from 29.30 to 30.36 $W^{-1}m^{-1}$ when $z < 0.61$ cm. When $z > 0.61$ cm, γ decreases monotonically and reaches the minimum value of 24.33 $W^{-1}m^{-1}$ at $z = 5.1$ cm. The ratio of the γ values at the input and the output ports is 1.20. Since the relative variation of $\gamma(z)$ is much lower than that of β_2, the nonlinearity variation can be considered as a perturbation to

Optics EXPRESS

the self-similar propagation, which will be discussed in the following section. The influence of nonzero α_0 will be also discussed.

4. Self-similar pulse compression in the waveguide taper

From Eq. (5), when the nonlinear coefficient is a constant and the dispersion coefficient decreases exponentially, a chirped soliton will be compressed exponentially as the ideal case described by Eq. (3). To study the self-similar pulse compression in the designed waveguide, we model the pulse propagation dynamics by using Eq. (3). The initial chirp factor $\xi = -9.87$ ps^{-2} according to Eq. (4). The full width at half maximum (FWHM) of the input hyperbolic secant pulse is 1 ps. With the initial dispersion $\beta_2(0) = -6.3628$ ps^2/m and nonlinearity $\gamma(0) = 29.30$ $W^{-1}m^{-1}$, the peak power is chosen as 0.67 W to satisfy the fundamental soliton condition according to Eq. (6). A compression factor F_c to describe the degree of compression is defined as

$$F_c = T_{\mathrm{FWHM\_i}} / T_{\mathrm{FWHM\_o}}, \tag{7}$$

where $T_{\mathrm{FWHM\_i}}$ and $T_{\mathrm{FWHM\_o}}$ are the FWHMs of the input and output pulses, respectively. In addition, a compression quality factor Q_c is used to quantify the compression performance as [7, 23]

$$Q_c = P_{\mathrm{out}} / (P_{\mathrm{in}} F_c), \tag{8}$$

where P_{out} and P_{in} are the peak powers of the output and input pulses, respectively.

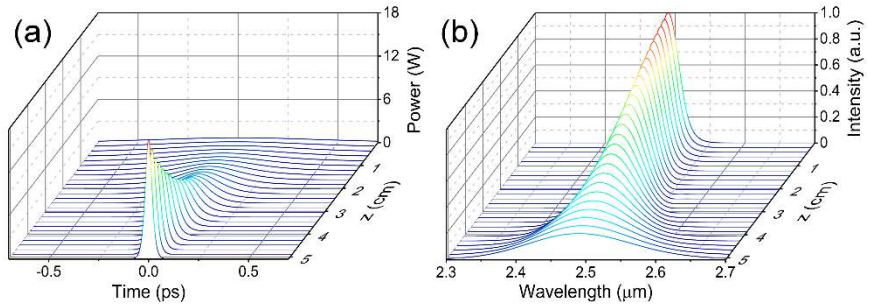

Fig. 3. The evolutions of the (a) temporal waveform and (b) normalized spectrum of the pulse along the propagation distance in the waveguide in the ideal case, where the variation of $\gamma(z)$, α_0, 3PA, HON, and HOD are all neglected.

Figures 3(a) and 3(b) respectively show the evolutions of the temporal profile and normalized spectrum of the pulse along propagation distance in the waveguide in the ideal case without considering the variation of $\gamma(z)$, α_0, 3PA, HON, and HOD. In the propagtaion, the input pulse is exponentially compressed and the temporal profile is kept as hyperbolic secant. In the pulse compression process, the temporal and spectral profiles are both symmetric without pedestal or satellitic peaks. After compression, T_{FWHM} and peak power of the output pulse are 40.62 fs and 16.61 W, respectively. According to Eqs. (8) and (9), F_c and Q_c of self-similar pulse compression in the designed waveguide taper in ideal case are 24.62 and 1, respectively.

However, the impacts of the variation of $\gamma(z)$, α_0, 3PA, HON, and HOD cannot be ignored in realistic case. Figures 4(a) and 4(b) show the evolutions of the temporal pulse and normalized output spectrum along propagation distance in the waveguide when the variation of $\gamma(z)$, α_0, 3PA, HON, and HOD are all considered. α_0 is chosen as 0.026 dB/cm [41–43] and the 3PA coefficient $\gamma_{3\mathrm{PA}}$ is 0.028 cm^3/GW^2 [30]. HOD coefficients are considered up to 6-th order. The input pulse is same as that used in the ideal case. The evolutions shown in Figs. 4(a) and 4(b) are similar to the ideal case but with longer pulse durations, lower intensities

Optics EXPRESS

and narrower bandwidths. At the output port of the waveguide taper, the 1-ps input pulse is compressed to 57.29 fs corresponding to an F_c of 17.46, which is lower than the designed F_c 24.62. The peak power of the output pulse is 10.63 W. The corresponding Q_c is 0.91.

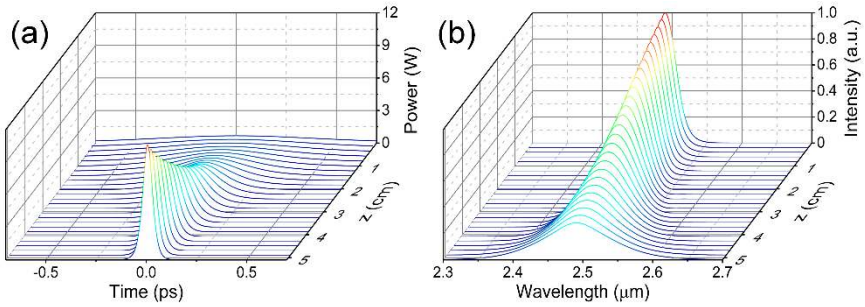

Fig. 4. The evolutions of the (a) temporal profile and (b) normalized spectrum of the pulse along the propagation distance in the waveguide when the variation of $\gamma(z)$, α_0, 3PA, HON, and HOD are all considered.

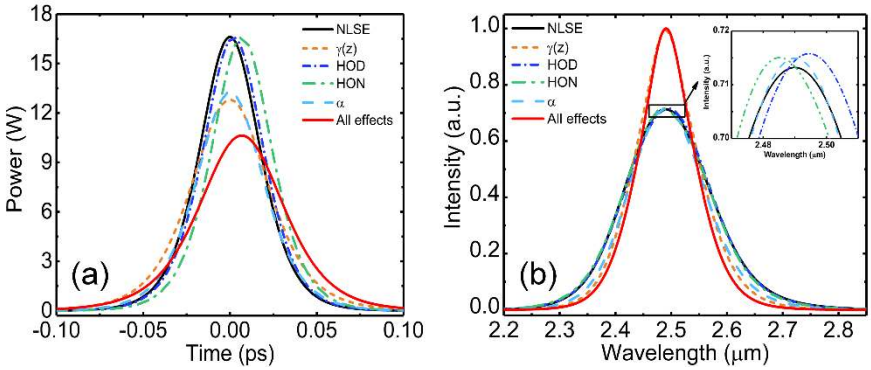

Fig. 5. Comparison of (a) the temporal profiles and (b) normalized spectra of the output pulses when the variation of $\gamma(z)$ (orange short dashed curves), α including α_0 and 3PA (cyan dashed curves), HON (green dash dotted curves) which means the self-steepening, and HOD (blue short dash dotted curves) are considered, respectively. The output pulse of the ideal case (NLSE, black solid curves) and realistic case with all effects included (red solid curves) are also plotted for comparison. The inset in (b) shows the detail of the peaks in the curves of NLSE, HON, HOD, and α.

Clearly, the inclusion of the multiple effects have deviated the pulse propagation from the ideal self-similar pulse compression. To characterize the impact of each effect to perturb the self-similar pulse compression, we compare the pulse propagation with the inclusion of each effect respectively. Figures 5(a) and 5(b) show the comparison of the temporal waveforms and normalized output spectra of the output pulse when the variation of $\gamma(z)$, combined losses α including the linear loss α_0 and 3PA, HON, and HOD are respectively considered. The outputs in the ideal case and realistic case with all effects are also plotted for comparison. From Figs. 5(a) and 5(b), both the HOD and HON have slightly delayed the waveform by a few femtoseconds but the spectra are almost unchanged. In contrast, the peak power of waveform is greatly lowered to 12.81 W by the variation of $\gamma(z)$ and the compressed pulse duration is enlarged to 52.07 fs. The spectrum is accordingly narrowed. The lossy effect including α_0 and 3PA decreases the peak power to 13.27 W and simultaneously increases the pulse duration to 45.53 fs. Because of the energy loss, the peak of spectrum is not increased along the narrowing of spectrum. On the whole, the deviation of the pulse compression from the ideal self-similar propagation is mainly caused by the variation of $\gamma(z)$, linear loss, and 3PA.

Optics EXPRESS

Compared with the significant distortion caused by the HOD in [23], the impact of HOD is greatly reduced in our design as shown in Fig. 5. To quantify the contribution of HOD in the self-similar pulse compression, we plot the different order dispersion lengths, L_{Dk} (k = 2, 3, 4, and 5) for comparison, as shown in Fig. 6, where L_{Dk} is defined as

$$L_{Dk}(z) = T_0^k(z) / |\beta_k(z)|, \tag{9}$$

where $T_0(z)$ is the pulse width and $\beta_k(z)$ is k-th order dispersion coefficient at propagation distance z. The ratio $L_{D2}/L_{D3} = |\beta_3/(\beta_2 T_0)|$ to estimate the relative contribution of third order dispersion, is also plotted in Fig. 6. Along the propagation, L_{D2} and L_{D3} both decrease monotonically since the spectrum of the pulse is increasing. Although the relative contribution $|\beta_3/(\beta_2 T_0)|$ also increases monotonically, the maximum $|\beta_3/(\beta_2 T_0)|$ is less than 0.6, which indicates a weak impact of β_3 in the whole propagation process. In addition, β_4 and β_5 are zero at z = 0.19 and 1.28 cm, which lead to infinite values of L_{D4} and L_{D5}. The values of L_{D4} and L_{D5} are much larger than L_{D2}, hence the effects of β_4 and β_5 are much weaker than that of β_2. It can be concluded that choosing a region of flat dispersion far from the ZDW has greatly reduced the distortion induced by HOD in the self-similar propagation.

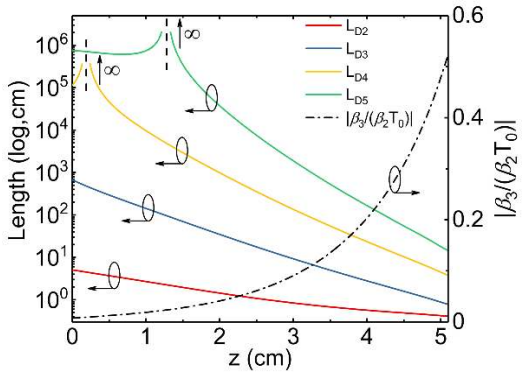

Fig. 6. The variations of different order dispersion lengths L_{Dk} (k = 2, 3, 4 and 5, red, navy, yellow, and green solid curves, respectively), and the ratio L_{D2}/L_{D3} (black dash dotted curve) along the propagation distance. The black dashed vertical lines indicate the locations with zero β_4 and β_5.

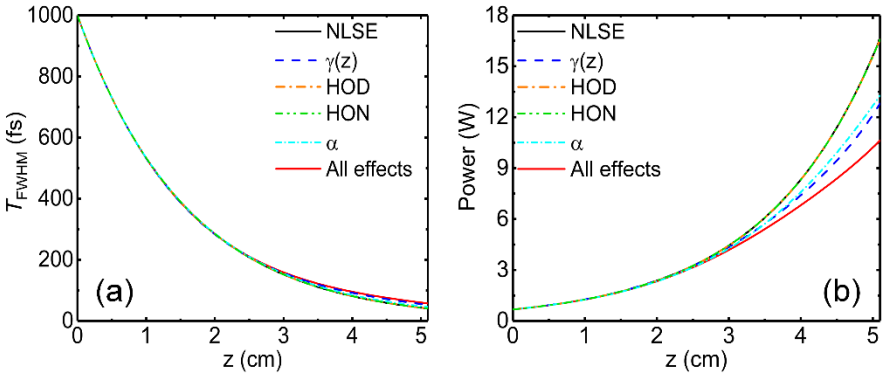

Fig. 7. The evolutions of (a) T_{FWHM} and (b) the peak power of the pulse along the propagation in the waveguide taper in the ideal case (NLSE, black solid curves), with the variation of $\gamma(z)$ (blue dashed curves), HOD (orange dash dotted curves), HON (green dash dot doted curves), α including α_0 and 3PA (cyan short dash dotted curves), and all effects (red solid curves), respectively.

Figure 7 shows the evolutions of T_{FWHM} and the peak power of the pulse along the compression for the different cases shown in Fig. 5. The curves with HOD and HON overlap

Optics EXPRESS

well to the curve modeled by NLSE in the ideal case. In the region of z < 2.35 cm, the deviations of other curves from the ideal case are hard to observe. The deviations of the curves with the variation of $\gamma(z)$, lossy terms and all effects grow quickly and monotonically after the point of z = 2.35 cm. Clearly, either the decreasing nonlinear coefficient $\gamma(z)$ or the attenuated peak power will weaken the nonlinear effect to be insufficient to compensate the dispersion effect. Since the self-similar propagation condition is not satisfied, the pulse compression is degraded manifested as the increase of T_{FWHM} and decrease of the peak power at the output port. With the variation of $\gamma(z)$, T_{FWHM} and peak power of the output pulse are 52.07 fs and 12.81 W, which deviate from the ideal case by 11.45 fs and 3.80 W, respectively. The inclusion of the lossy terms increases T_{FWHM} by 16.67 fs to 57.29 fs and decreases the peak power by 5.98 W to 10.63 W, respectively.

From Fig. 7, any effects that perturb the self-similar propagation condition will degrade the quality of pulse compression and lead to output pulses with longer durations and lower peak powers. It is the ideal case that the pulse is a fundamental soliton at every point in the propagation with $L_{D2}(z) = L_{NL}(z)$ for all z values, where $L_{NL}(z) = 1/[\gamma(z)P_0(z)]$ is the nonlinear length. Figures 8(a) and 8(b) show the variations of L_{D2} and L_{NL} along the propagation in the waveguide taper for different cases to evaluate the quality of self-similar propagation. The chirp length $L_C = 1/\sigma$ is plotted to estimate the contributions of dispersion and nonlinearity effects in self-similar compression process [44]. The lengths are plotted in logarithmic scale for better presentation of the differences. In Fig. 8(c), the relative separations of L_{D2} and L_{NL}, $\delta L/L = 2(L_{D2}-L_{NL})/(L_{D2} + L_{NL})$ in cased with $\gamma(z)$ or all effects are plotted respectively. Because of the variation of $\gamma(z)$, both L_{D2} and L_{NL} deviate gradually from the ideal self-similar propagation. When all effects are included, similar but larger deviations are observed for both L_{D2} and L_{NL}, as shown in Fig. 8(b). However, the relative difference between L_{D2} and L_{NL} is less than 8% in the propagation of all cases, as shown in Fig. 8(c). Therefore, the fundamental soliton is still well maintained in the pulse compression process, and a much better output pulse quality is obtained compared with reported results in [23].

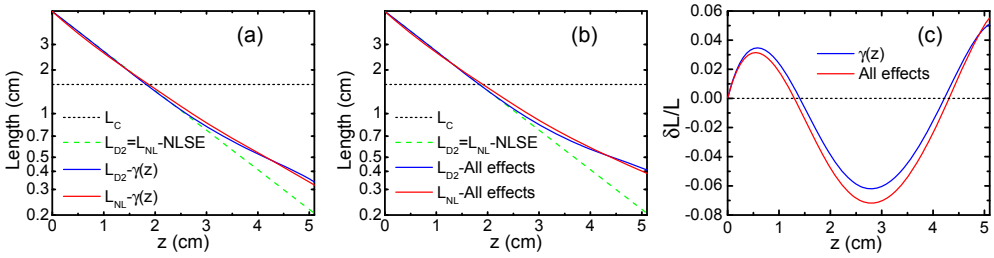

Fig. 8. The evolutions of the second-order dispersion length L_{D2} (red solid curves) and nonlinear length L_{NL} (blue solid curves) in logarithmic scale along the propagation in the waveguide taper when (a) only the variation of $\gamma(z)$ and (b) all effects are considered. The black dotted lines are the chirp length L_C. The green dashed curves represent L_{D2} and L_{NL} in the ideal case (NLSE) for comparison. (c) The relative deviations $\delta L/L = 2(L_{D2}-L_{NL})/(L_{D2} + L_{NL})$ in the cases with γ(z) or all effects included.

From the above discussions, the energy loss caused by α_0 and 3PA is the second important effect that deviate the self-similar pulse compression from the ideal case besides the variation of $\gamma(z)$. The 3PA coefficient is determined by the material and mode field size, which are fixed once the device is designed. However, α_0 may vary significantly depending on the fabrication techniques of the waveguide, which should be investigated in practice. The scattering by voids, damages and rough surfaces of the waveguide, along with the material absorption, are the dominant sources of loss [41]. With well-designed cross-section of the waveguide and optimized lithography and dry etching processes to reduce the sidewall roughness, α_0 can be reduced to 0.274 dB/cm [45]. With a combination of resist reflowing to form a surface-tension confined smooth etch mask and a low DC bias dry etch to reduce

Optics EXPRESS

roughness and damage in the silicon sidewalls, α_0 can be further reduced to 0.1 dB/cm [46]. By using the passive-split wafers, an α_0 as low as 0.026 dB/cm was measured [42]. We characterize the self-similar pulse compression with α_0 = 0.026, 0.1, 0.274, and 1 dB/cm by the evolutions of T_{FWHM} and peak power of the pulse, as shown in Fig. 9. The case with zero α_0 is also plotted for comparison. In Fig. 9, although the input pulses are all compressed along the propagation in the waveguide taper, the output pulses, especially the peak powers of them, are significantly affected by α_0. Table 1 summarizes the parameters T_{FWHM}, peak power, and F_c of the output pulses with different α_0. When a large α_0 = 1 dB/cm is adopted, the peak power of the pulse is increased but then decreased at the final stage of propagation, which is clearly no longer a self-similar propagation. Thus, from Fig. 9 and Table 1, a low α_0 will lead to perturbation to the self-similar pulse compression but a large enough α_0 will eventually destroy the self-similar propagation.

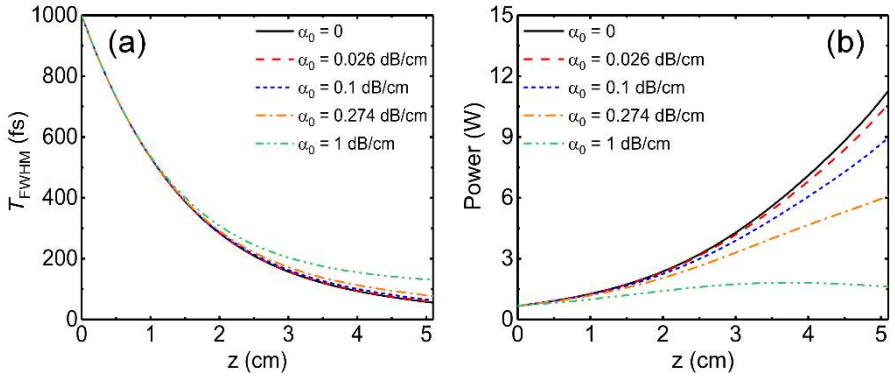

Fig. 9. The evolutions of (a) T_{FWHM} and (b) peak power of the pulses along the propagation in the waveguide taper with α_0 = 0.026 (red dashed curves), 0.1 (blue short dashed curves), 0.274 (orange dash dotted curves), and 1 dB/cm (green dash dot dotted curves), respectively. The curves for α_0 = 0 (black solid curves) are also plotted for comparison.

Table 1. T_{FWHM}, peak power, and F_c of the output pulse for different α_0 and a 1-ps input pulse.

α_0 (dB/cm)	T_{FWHM} (fs)	Peak power (W)	F_c
0	55.43	11.27	18.04
0.026	57.29	10.63	17.46
0.1	62.92	8.97	15.89
0.274	77.23	6.08	12.94
1	130.44	1.62	7.67

In the above discussion, we have considered the perturbations to the self-similar propagation coming from the practical taper parameters with a 1-ps input pulse. The designed waveguide taper is applicable to compress pulses with different durations by a fixed compression ratio, while the peak power should be varied simultaneously to satisfy the fundamental soliton condition. Considering the perturbations of HODs and self-steepening, a longer input pulse with a lower peak power will have a better compression quality since the bandwidth is narrower. The self-similar pulse compression will be always valid unless the input pulse spectrum is too broad that the HOD and HON will significantly degrade the compression.

Optics EXPRESS

5. Conclusion

In summary, we design a simple inversely tapered silicon ridge waveguide with exponentially decreasing dispersion profile to achieve mid-infrared self-similar pulse compression of low power picosecond pulse. In the designed waveguide taper, a 1-ps input pulse at the wavelength of 2490 nm is successfully compressed to 57.29 fs in only 5.1-cm propagation, along with an F_c of 17.46. We study the impacts of HOD, HON, α, and the variation of $\gamma(z)$ on the pulse compression process. Compared with the HOD and HON, α and variation of $\gamma(z)$ are considered as the dominant perturbations to degrade the self-similar pulse compression. In future work, the performance of the self-similar pulse compression can be further enhanced through optimizing the nonlinear parameter of the silicon waveguide taper and reducing α_0 during the fabrication process. Our proposed inversely tapered silicon ridge waveguide is simple and easy to fabricate, and should have immediate interest for realization of on-chip ultrashort pulse sources for nonlinear photonics and spectroscopy in the mid-infrared spectral region.

Funding

National Natural Science Foundation of China (NSFC) (61475023 and 61475131); Beijing Youth Top-notch Talent Support Program (2015000026833ZK08); Natural Science Foundation of Beijing (4152037); Fund of State Key Laboratory of Information Photonics and Optical Communications (Beijing University of Posts and Telecommunications) China (IPOC2016ZT05 and IPOC2017ZZ05); Shenzhen Science and Technology Innovation Commission (JCYJ20160331141313917); Research Grant Council of Hong Kong (PolyU152144/15E and PolyU152471/16E).